Supporting Information

Radiation-responsive scintillating nanotheranostics for reduced hypoxic radioresistance under ROS/NO-mediated tumor microenvironment regulation

Yan Dou[1], Yajuan Liu[2], Fangshi Zhao[1], Yanyan Guo[3], Xue Li[3], Menglin Wu[3], Jin Chang[2], and Chunshui Yu[1]

Address correspondence to E-mail: chunshuiyu@tijmu.edu.cn

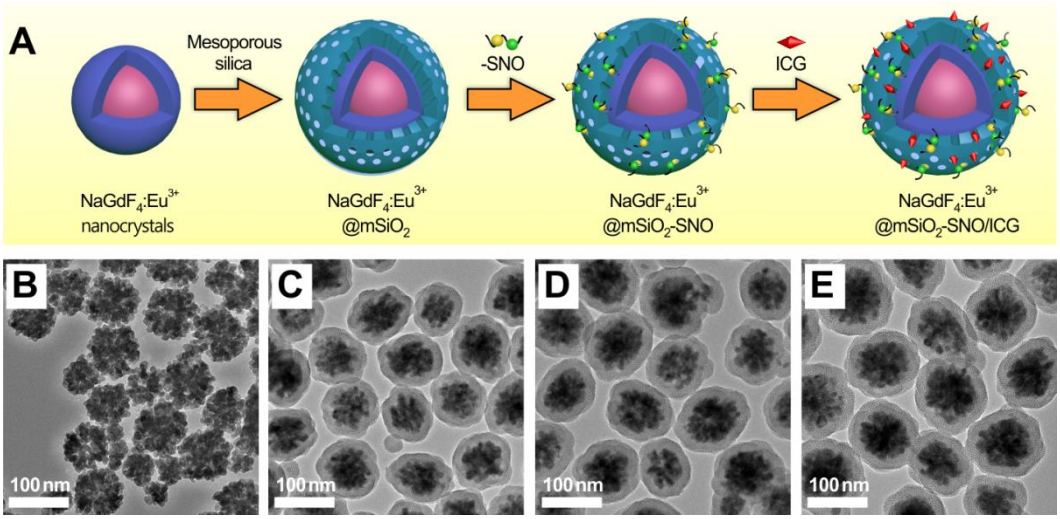

Figure S1. (A) Schematic of NSC@mSiO$_2$-SNO/ICG NPs synthesis route. **(B-E)** TEM images: NSC NPs **(B)**, NSC@mSiO$_2$ NPs **(C)**, NSC@mSiO$_2$-SNO NPs **(D)** and NSC@mSiO$_2$-SNO/ICG NPs **(E)**.

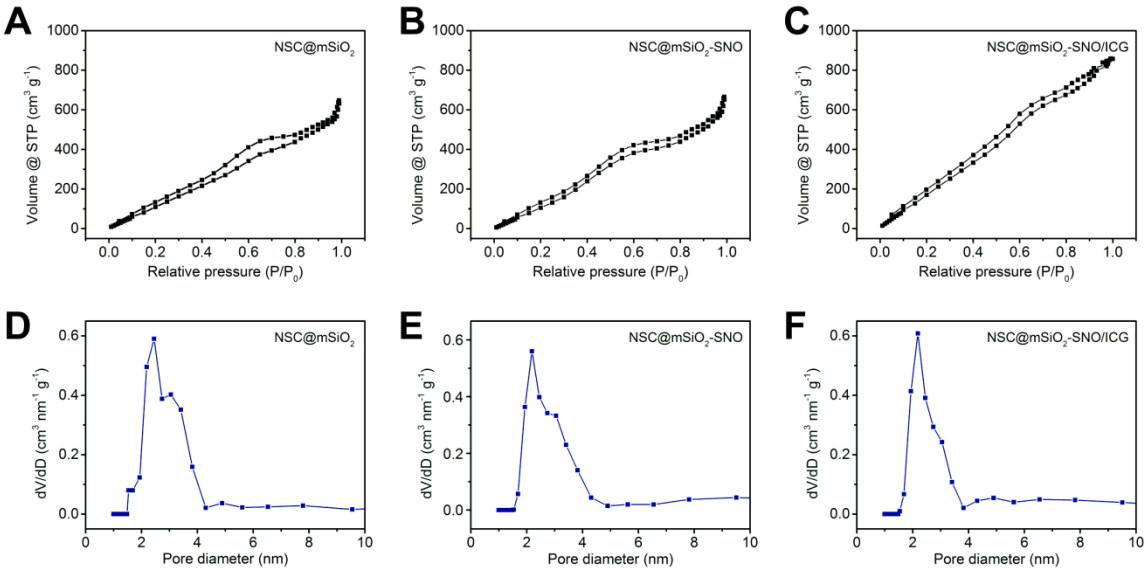

Figure S2. (**A-C**) Nitrogen adsorption-desorption isotherms and (**D-F**) pore size distribution curves of NSC@mSiO$_2$ NPs, NSC@mSiO$_2$-SNO NPs and NSC@mSiO$_2$-SNO/ICG NPs.

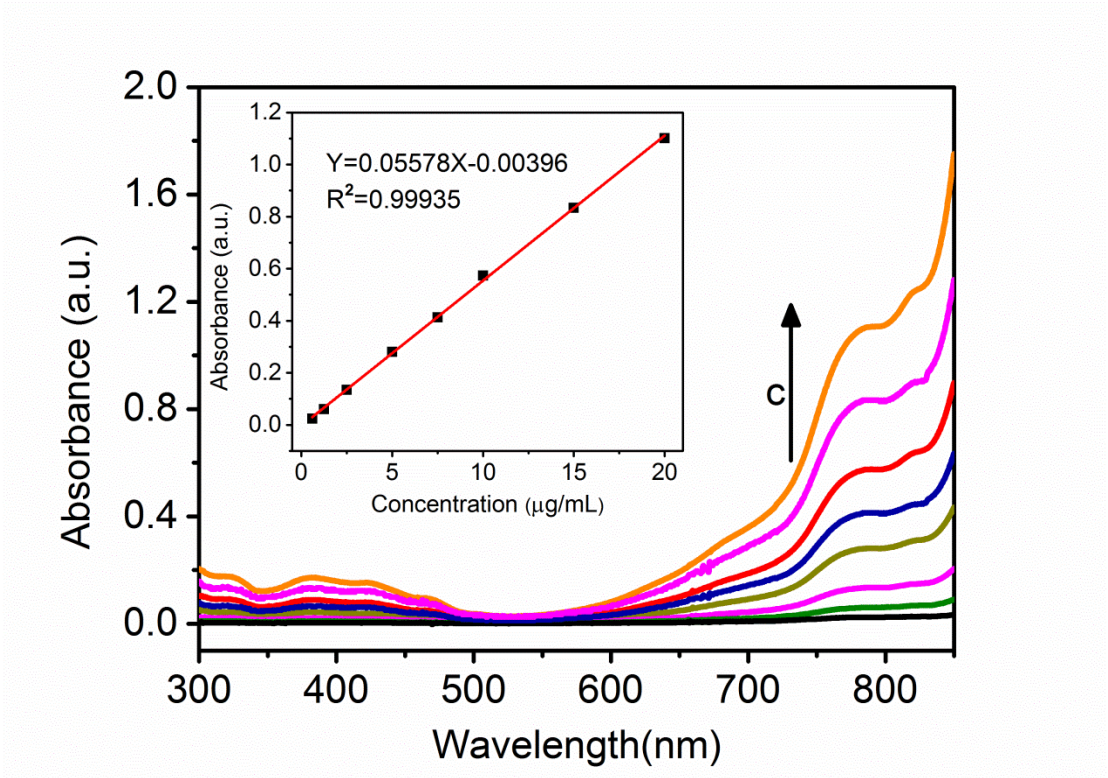

Figure S3. UV-vis-NIR absorption spectra of ICG at different concentrations. Insert: concentration-dependent elevation of ICG specific absorbing peak at 784 nm.

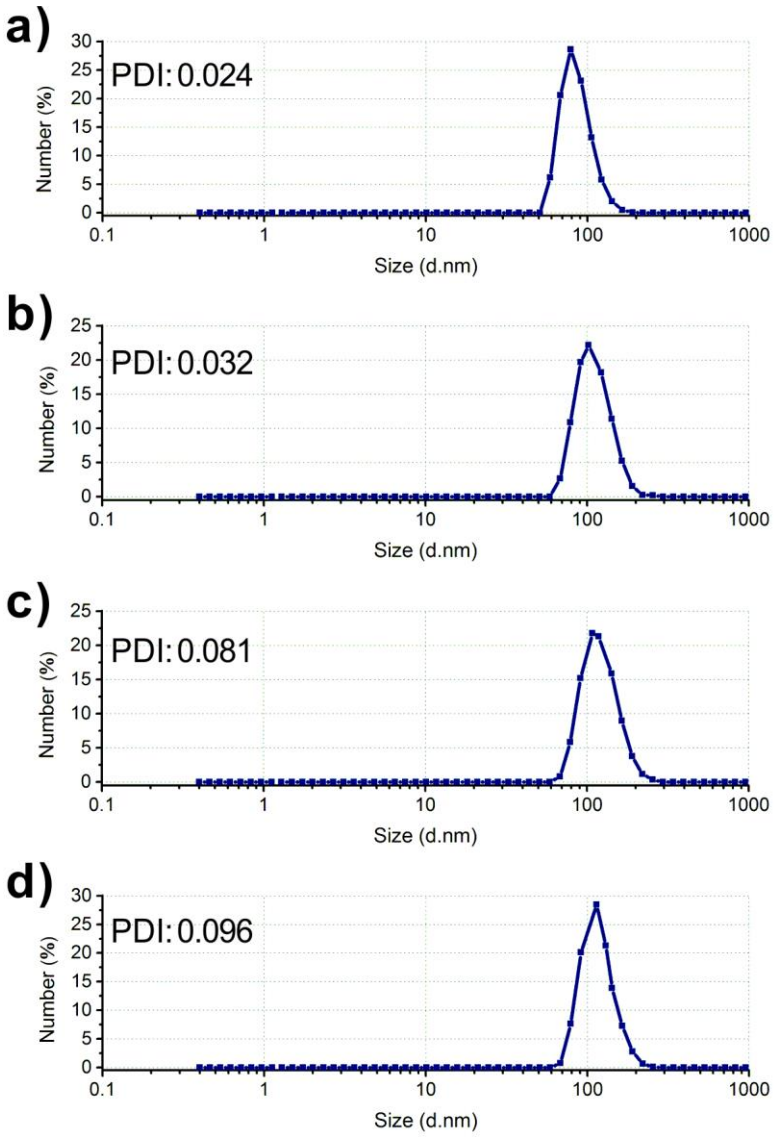

Figure S4. Dynamic light scattering (DLS) sizes and PDI values of NSC NPs **(A)**, NSC@mSiO$_2$ NPs **(B)**, NSC@mSiO$_2$-SNO NPs **(C)** and NSC@mSiO$_2$-SNO/ICG NPs **(D)** in DI water.

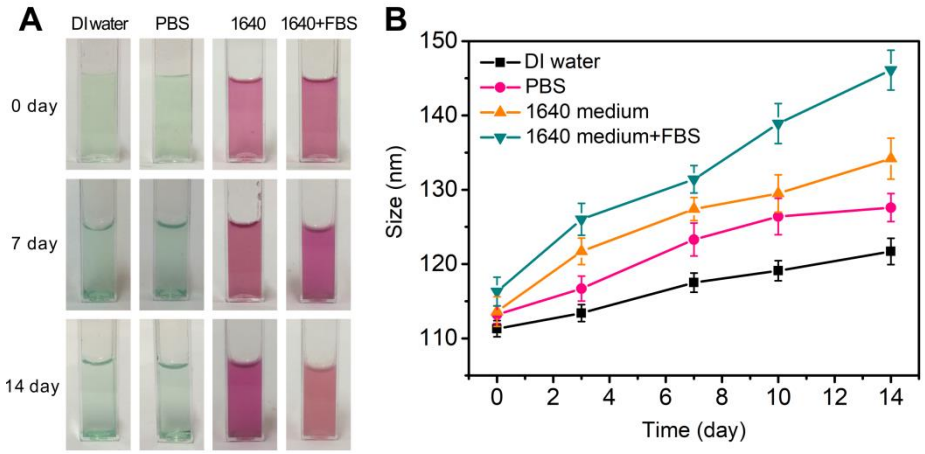

Figure S5. Colloidal stability of NSC@mSiO_2-SNO/ICG NPs. The photos (**A**) and corresponding DLS measured sizes (**B**) were recorded during 14 days, for incubation of various solutions including DI water, phosphate buffered saline (PBS), 1640 cell medium, and 1640 cell medium containing fetal bovine serum (FBS). Error bars indicate standard deviations (SD) (n=3).

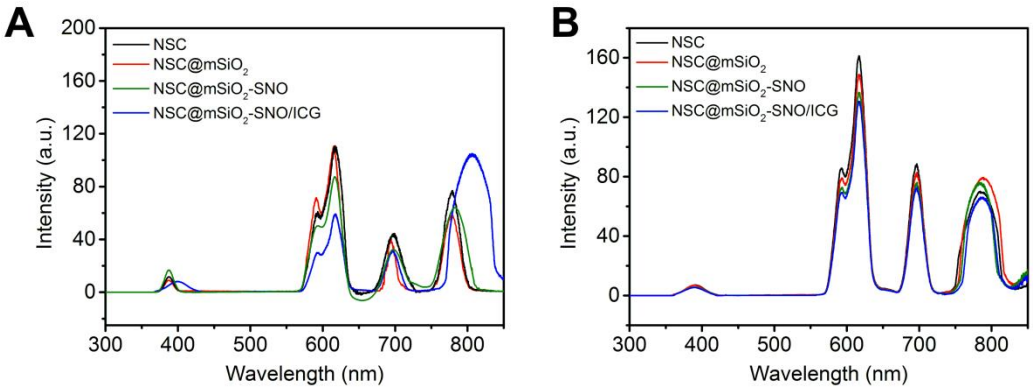

Figure S6. X-ray excited luminescence spectra **(A)** and UV-excited photoluminescence spectra **(B)**.

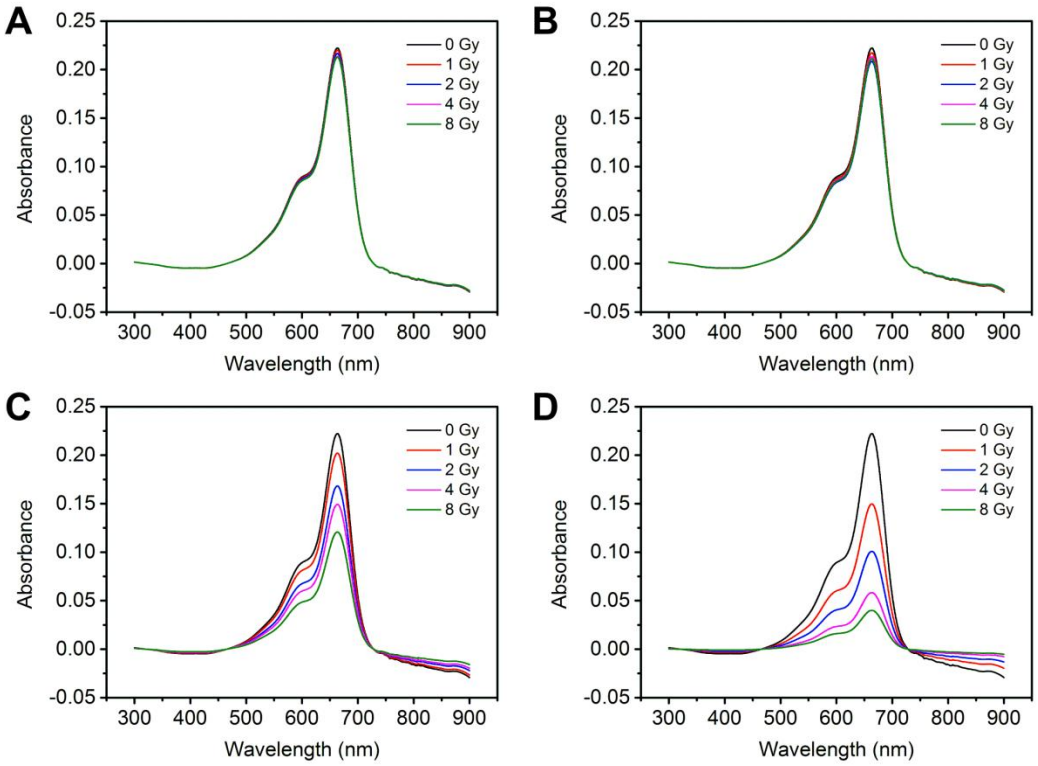

Figure S7. UV-vis-NIR absorption spectra of methylene blue (MB) solutions incubated with DI water **(A)**, pure ICG (2 μg/mL) **(B)**, NSC@mSiO_2-SNO **(C)** andNSC@mSiO_2-SNO/ICG **(D)** under different doses of X-ray radiations (0, 1, 2, 4, 8 Gy).

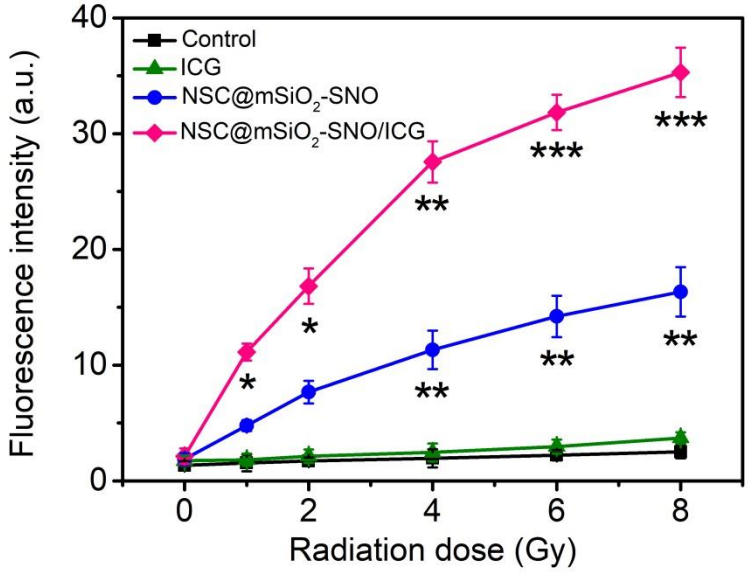

Figure S8. Fluorescence intensities measured at an excitation wavelength of 395 nm and emission wavelength of 442 nm to evaluate the production of ·OH by using 3-CCA.

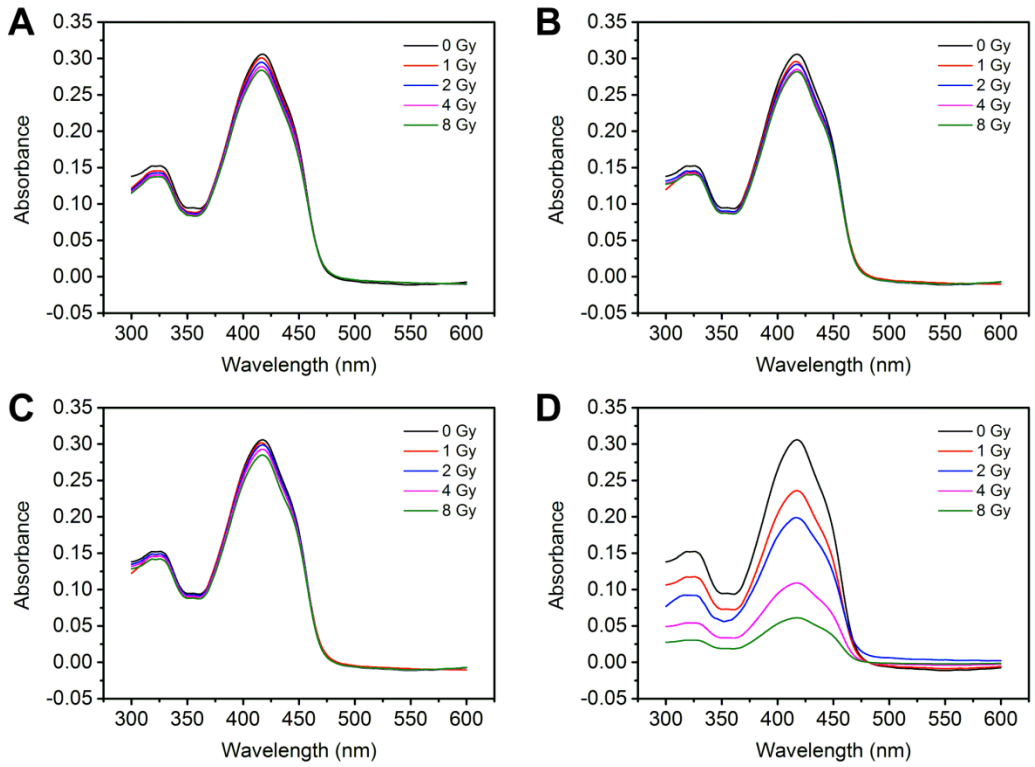

Figure S9. UV-vis absorption spectra of 1,3-Diphenylisobenzofuran (DPBF) solutions incubated with DI water **(A)**, pure ICG (2 μg/mL) **(B)**, NSC@mSiO_2-SNO **(C)** and NSC@mSiO_2-SNO/ICG **(D)** under different doses of X-ray radiations (0, 1, 2, 4, 8 Gy).

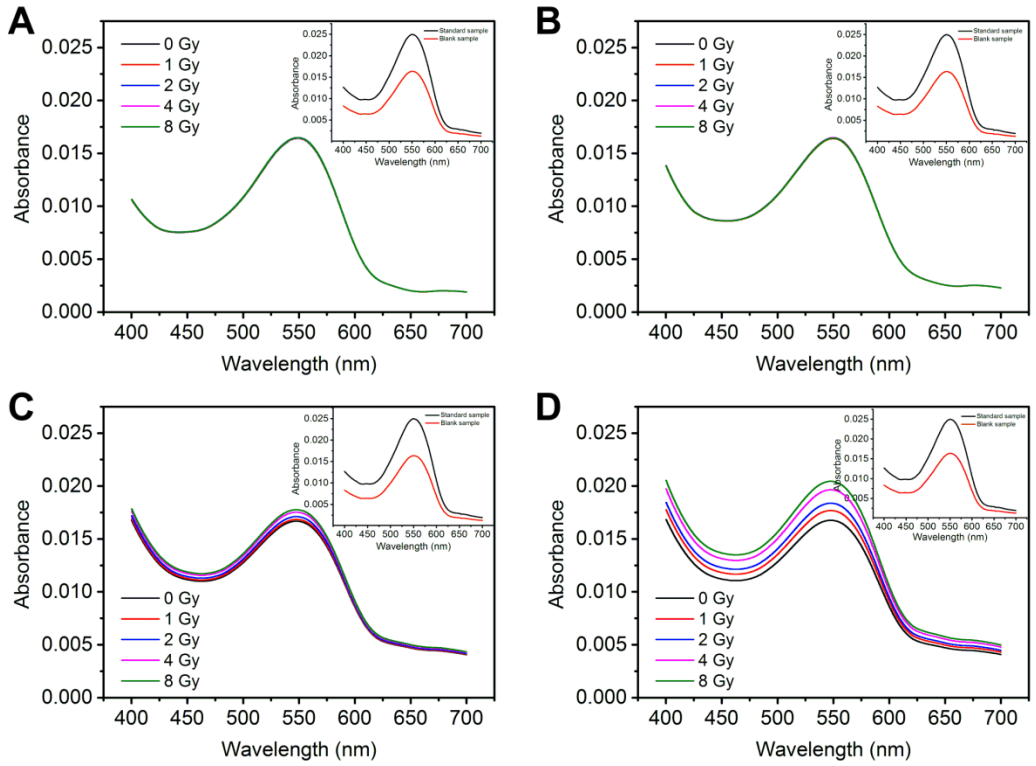

Figure S10. UV-vis-NIR absorption spectra of different solutions: DI water **(A)**, pure ICG (2 μg/mL) **(B)**, NSC@mSiO$_2$-SNO **(C)** and NSC@mSiO$_2$-SNO/ICG **(D)**, determined by a typical Griess assay after different doses of X-ray radiations (0, 1, 2, 4, 8 Gy). Insert: spectra of blank control and standard sample.

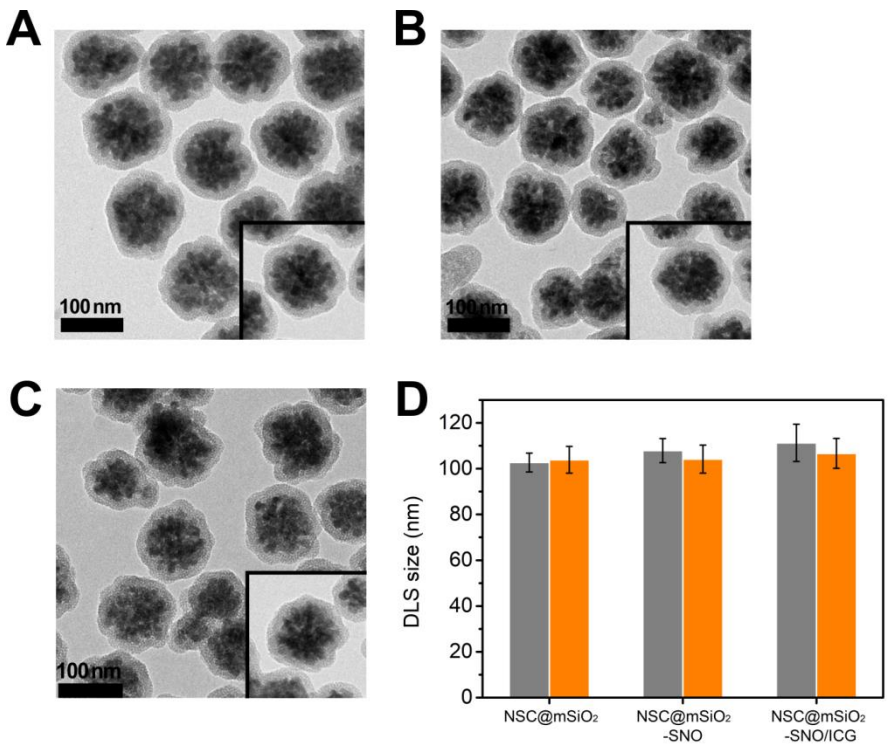

Figure S11. TEM images (**A-C**) and DLS sizes (**D**) of following nanoparticles after X-ray radiation with 4 Gy: NSC@mSiO_2 NPs **(A)**, NSC@mSiO_2-SNO NPs **(B)** and NSC@mSiO_2-SNO/ICG NPs **(C)**.

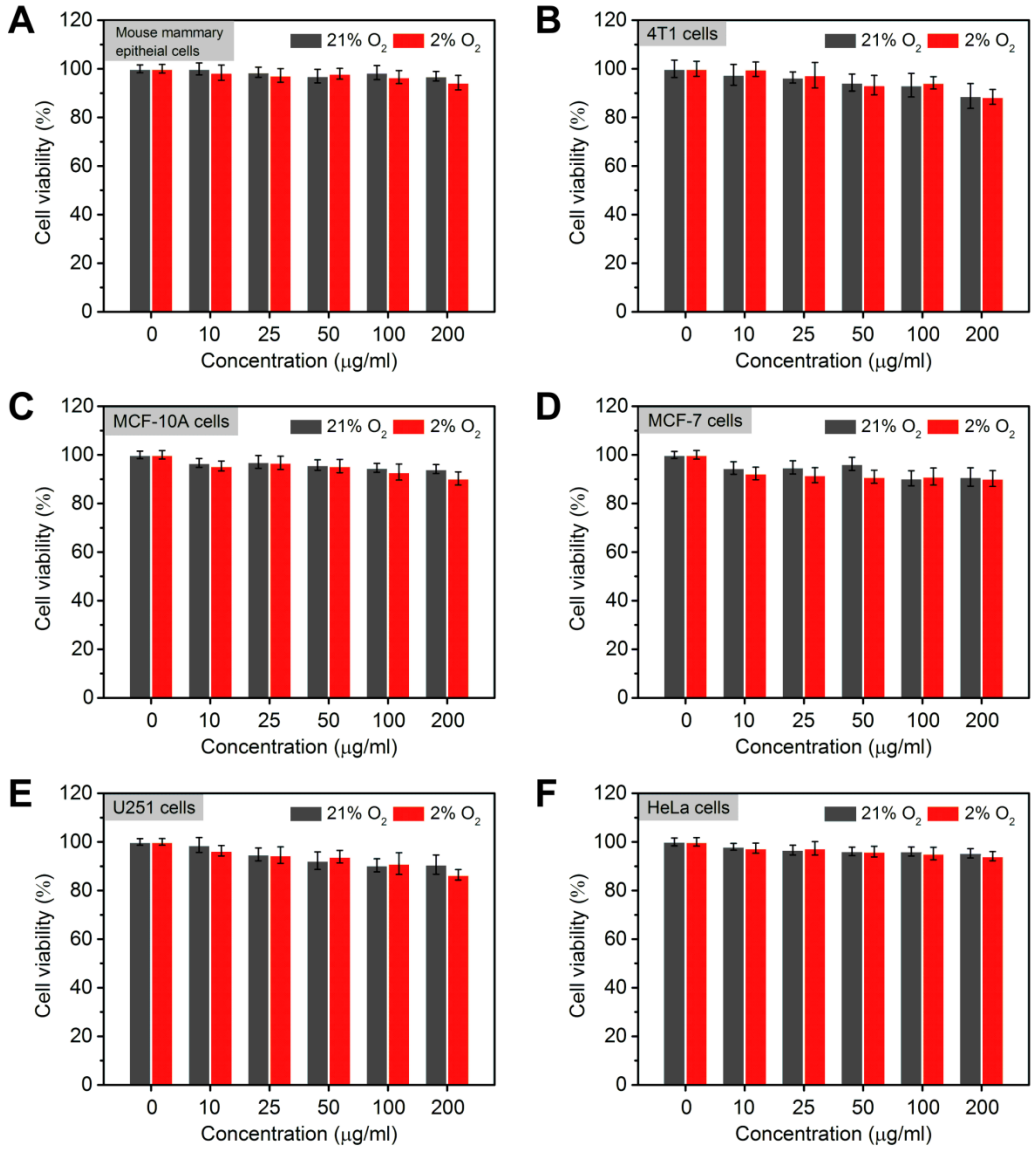

Figure S12. *In vitro* cytotoxicity of mouse mammary epithelial cells **(A)**, 4T1 cells **(B)**, MCF-10A cells **(C)**, MCF-7 cells **(D)**, U251 cells **(E)**, and HeLa cells **(F)** incubated with NSC@mSiO_2-SNO/ICG after 24 h normoxic (21% O_2) and hypoxic (2% O_2) culture. Error bars indicate standard deviations (SD) (n=5).

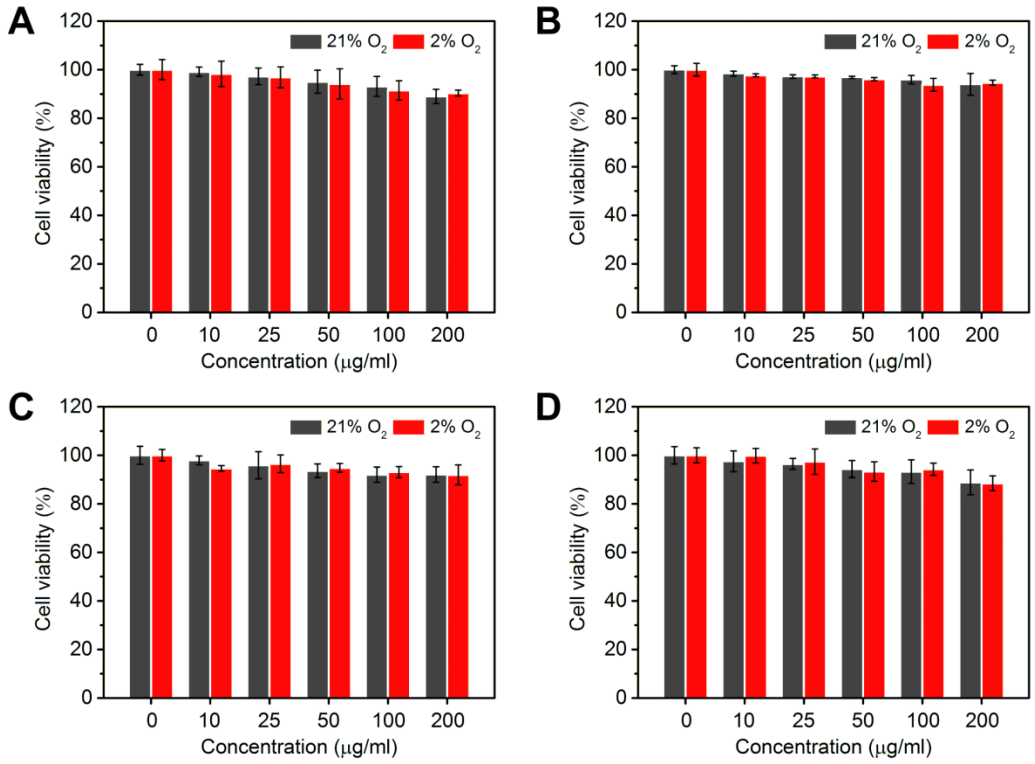

Figure S13. *In vitro* cytotoxicity of 4T1 cells incubated with NSC **(A)**, NSC@mSiO$_2$ **(B)**, NSC@mSiO$_2$-SNO **(C)** and NSC@mSiO$_2$-SNO/ICG **(D)** after 24 h normoxic (21% O$_2$) and hypoxic (2% O$_2$) culture. Error bars indicate standard deviations (SD) (n=5).

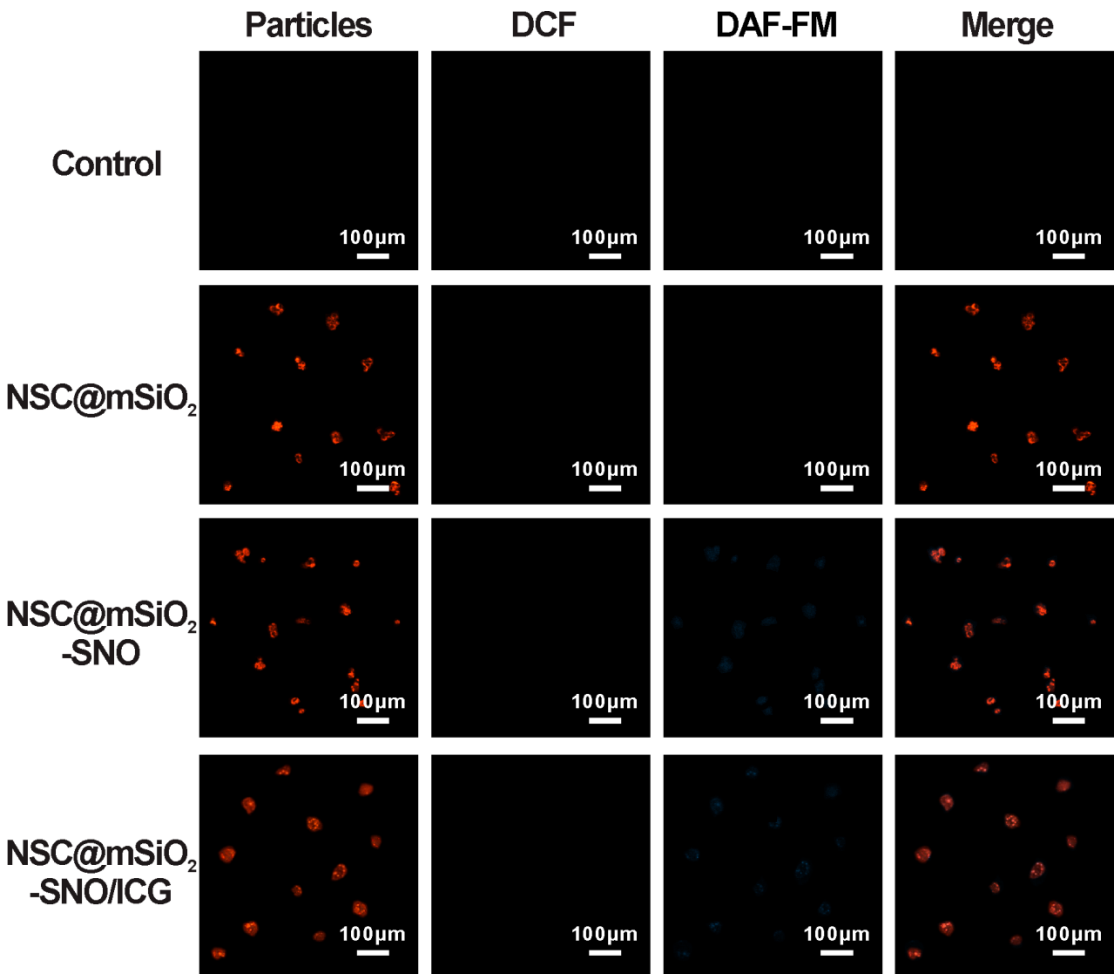

Figure S14. Confocal laser scanning microscopy (CLSM) images of ROS and NO generation in 4T1 cells incubated with control **(A)**, NSC@mSiO$_2$ **(B)**, NSC@mSiO$_2$-SNO **(C)** and NSC@mSiO$_2$-SNO/ICG **(D)** for 24 h. Green and blue luminescence indicate DAF-FM DA and DCFH-DA staining for ROS and NO, respectively. Red luminescence is emitted from NSC cores upon UV excitation. Scale bars, 100 μm.

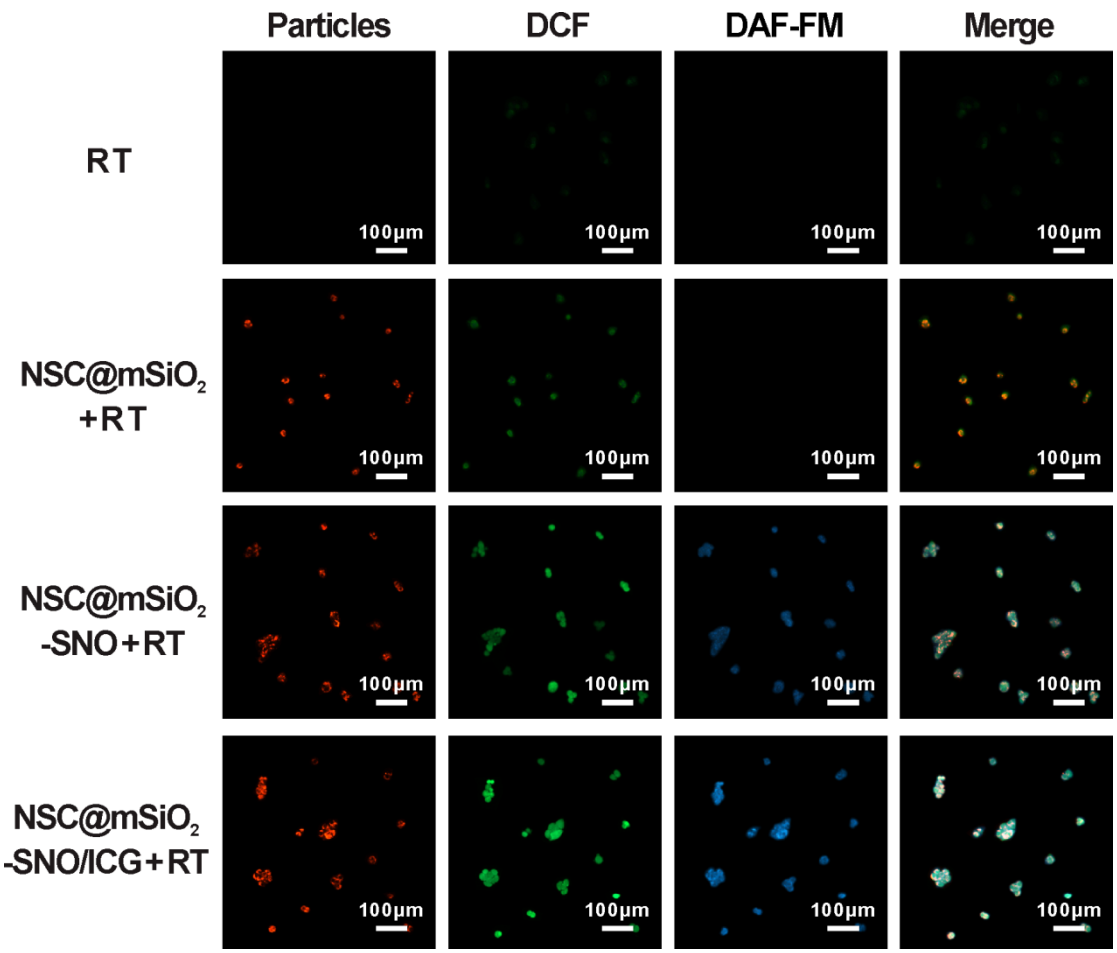

Figure S15. CLSM images of ROS and NO generation in 4T1 cells upon 4Gy X-ray radiation after hypoxic (2% O_2) incubation with control **(A)**, NSC@mSiO_2 **(B)**, NSC@mSiO_2-SNO **(C)** and NSC@mSiO_2-SNO/ICG **(D)** for 24 h. Green and blue luminescence indicate DAF-FM DA and DCFH-DA staining for ROS and NO, respectively. Red luminescence is emitted from NSC cores upon UV excitation. Scale bars, 100 μm.

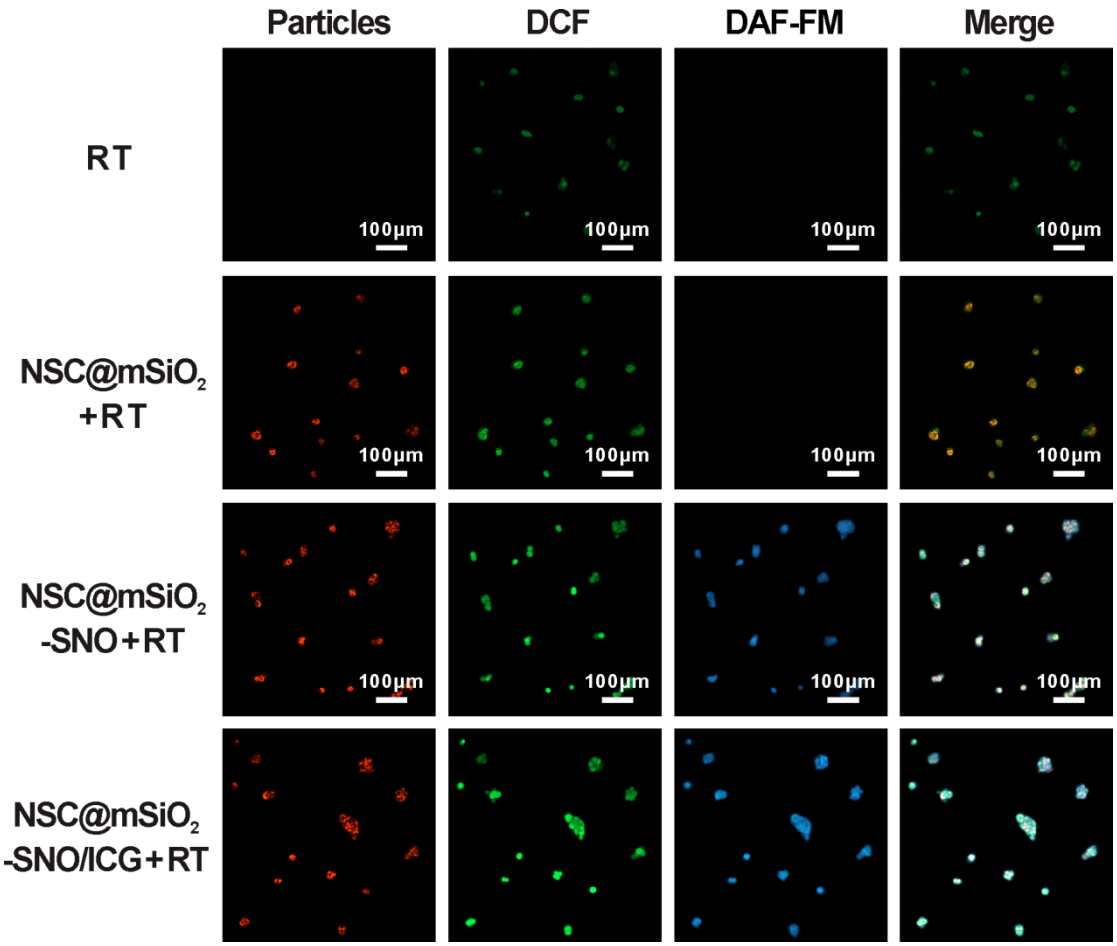

Figure S16. CLSM images of ROS and NO generation in 4T1 cells upon 4Gy X-ray radiation after normoxic (21% O_2) incubation with control **(A)**, NSC@mSiO_2 **(B)**, NSC@mSiO_2-SNO **(C)** and NSC@mSiO_2-SNO/ICG **(D)** for 24 h. Green and blue luminescence indicate DAF-FM DA and DCFH-DA staining for ROS and NO, respectively. Red luminescence is emitted from NSC cores upon UV excitation. Scale bars, 100 μm.

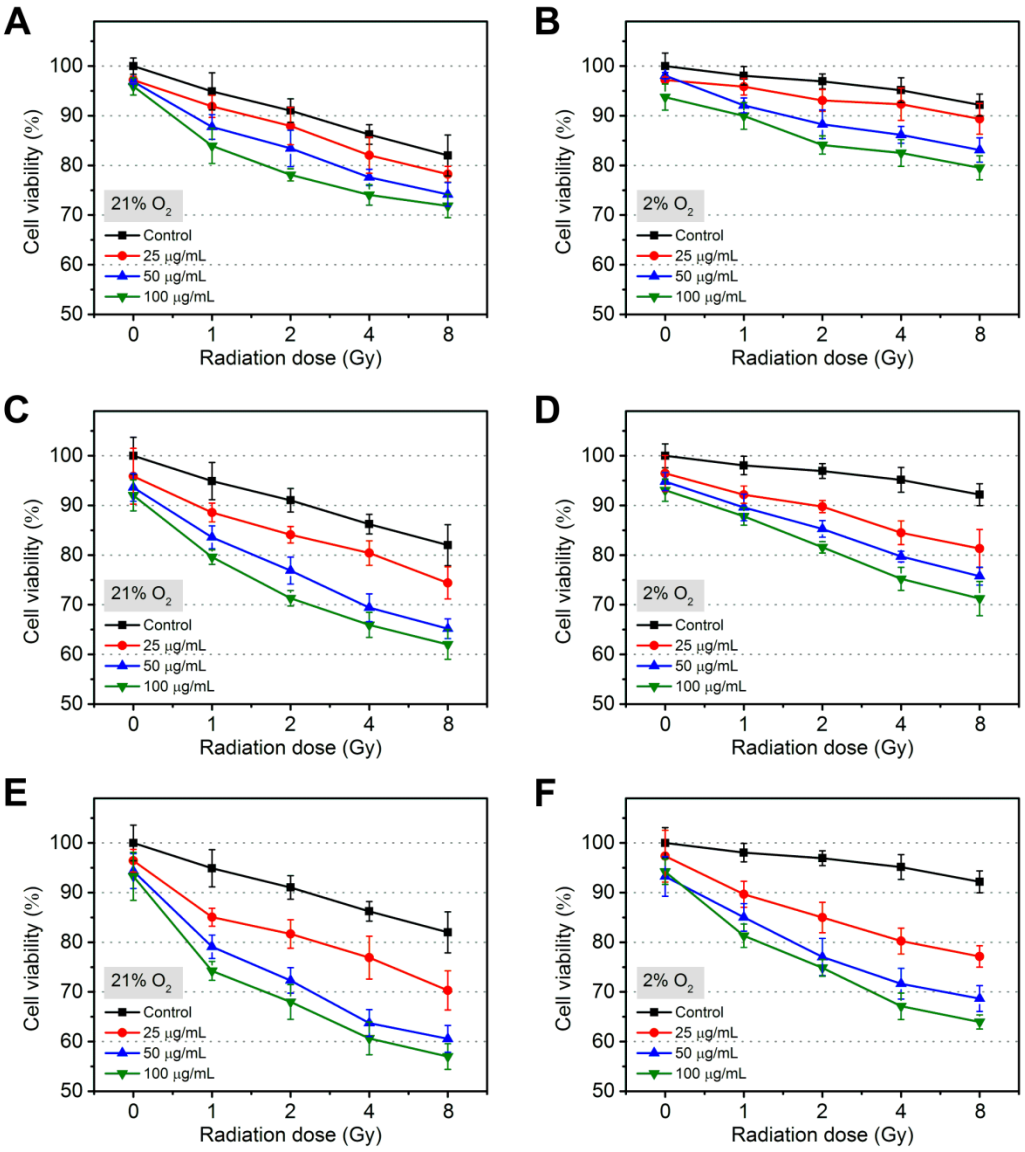

Figure S17. Cell viability of 4T1 cells treated with different concentrations of NSC@mSiO$_2$ **(A,B)**, NSC@mSiO$_2$-SNO **(C,D)** and NSC@mSiO$_2$-SNO/ICG **(E,F)** after 24 h normoxic (21% O$_2$: a,c,e) and hypoxic (2% O$_2$:b,d,f) culture followed by various doses of X-ray radiations (0, 1, 2, 4, 8 Gy). Error bars indicate standard deviations (SD) (n=3).

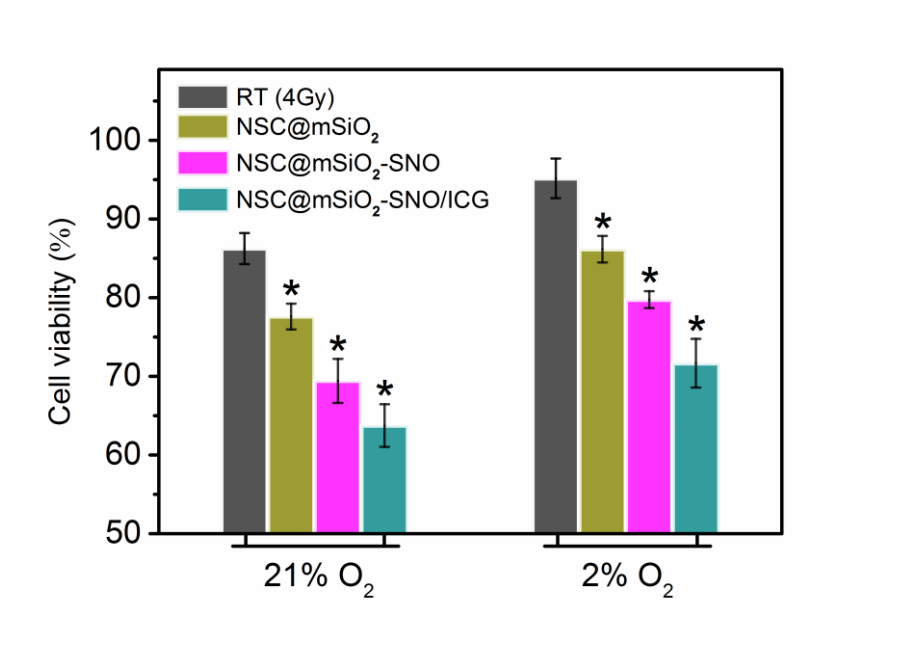

Figure S18. Cell viability (%) changes of 4T1 cells after different treatments.

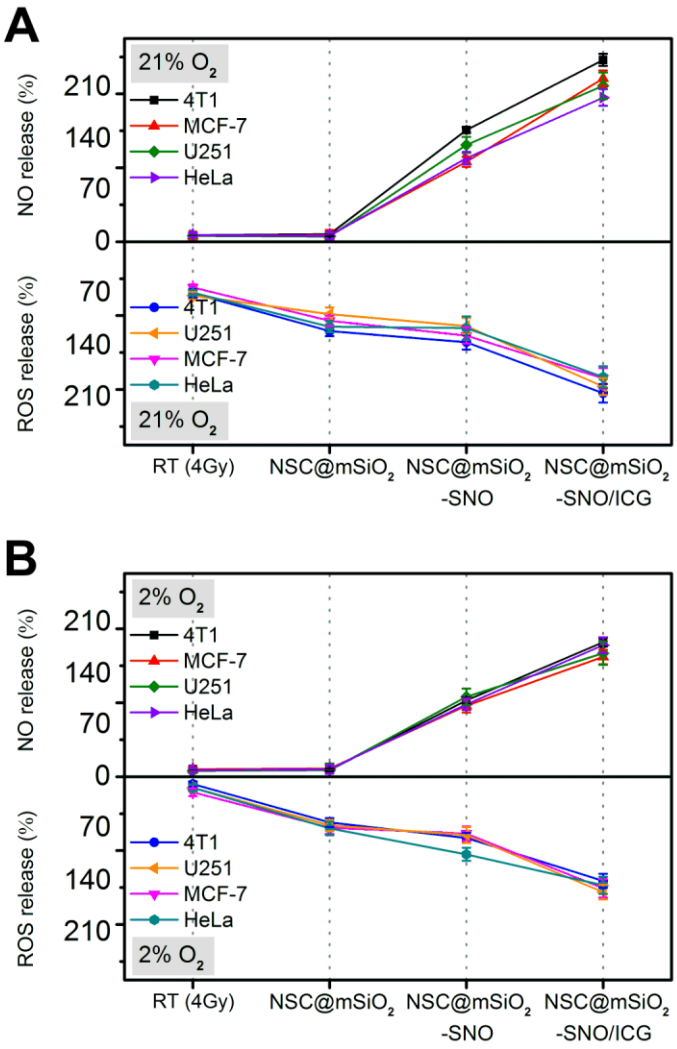

Figure S19. Quantitative intracellular ROS/NO production by flow cytometry for 4T1 cells, MCF-7 cells, U251 cells and HeLa cells after 24 h normoxic (21% O_2) **(A)** and hypoxic (2% O_2) **(B)** incubation with different NPs treatments at 50 μg/mL under 4 Gy X-ray radiation. Error bars indicate standard deviations (SD) (n=5).

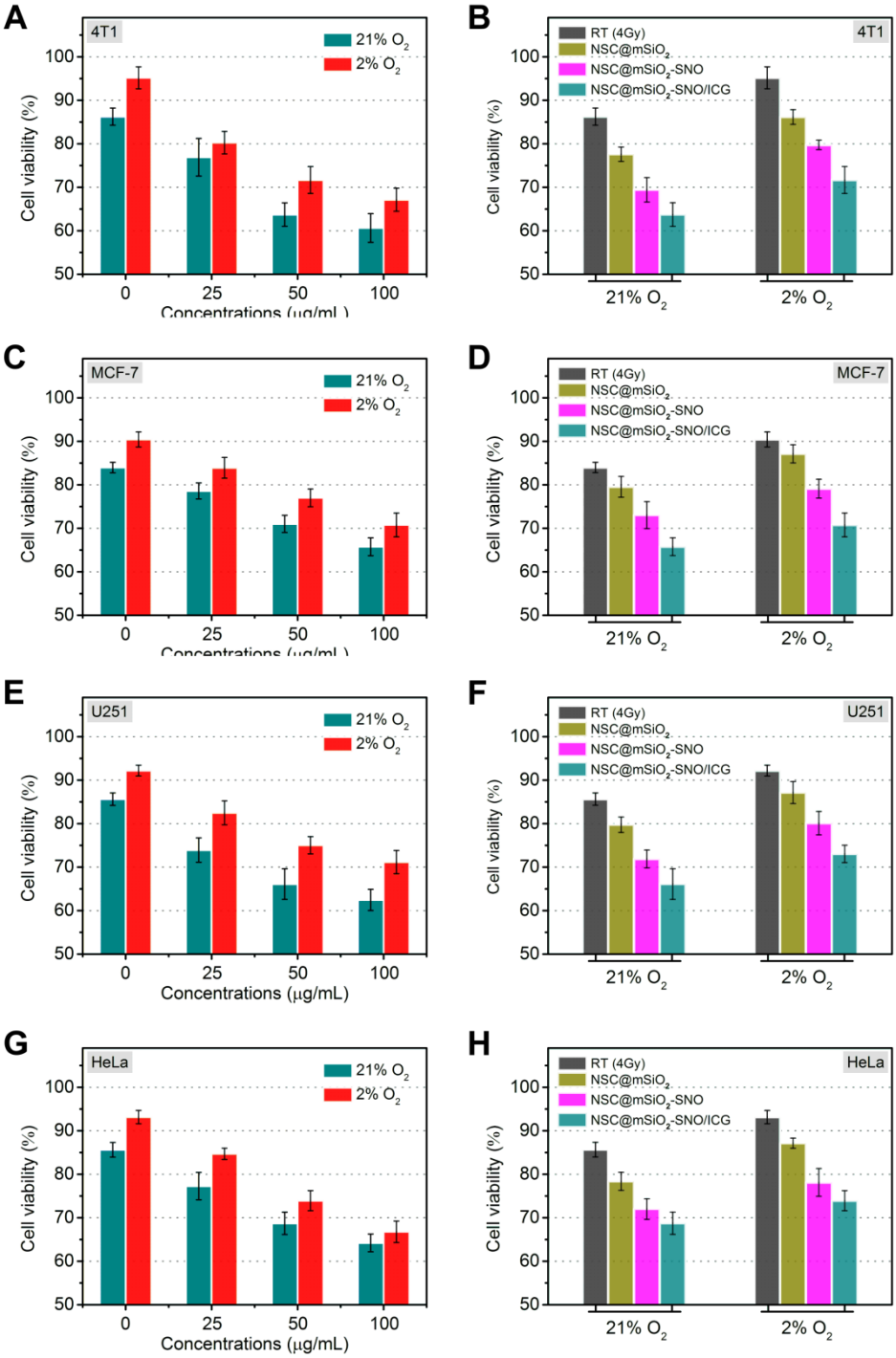

Figure S20. The evaluation of cancer cell selectivity for 4T1 cells **(A,B)**, MCF-7 cells **(C,D)**, U251 cells **(E,F)** and HeLa cells **(G,H)** by cell viability. (a,c,e,g) different concentrations of NSC@mSiO$_2$-SNO/ICG treatments under 4 Gy X-ray radiation. (b,d,f,h) Different NPs treatments at 50 μg/mL under 4 Gy X-ray radiation. Error bars indicate standard deviations (SD) (n=5).

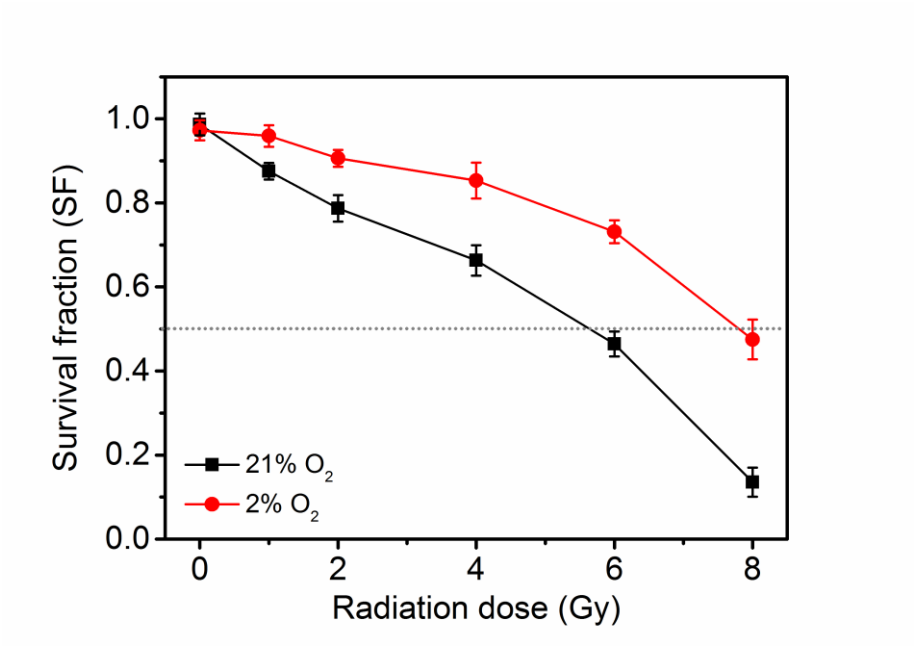

Figure S21. Clonogenic survival curves of 4T1 cells cultured under different oxygen pressures (pO_2) after X-ray radiation with doses ranging from 0 to 8 Gy.

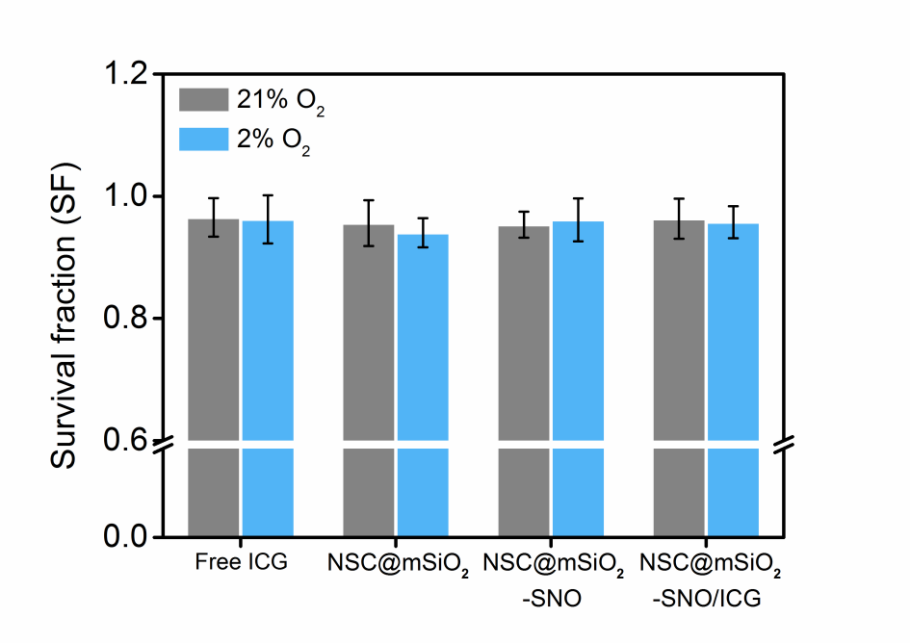

Figure S22. Survival fractions calculated from 4T1 cells after normoxic and hypoxic incubation with free ICG, NSC@mSiO2 NPs, NSC@mSiO2-SNO NPs, and NSC@mSiO2-SNO/ICG NPs for 24 h.

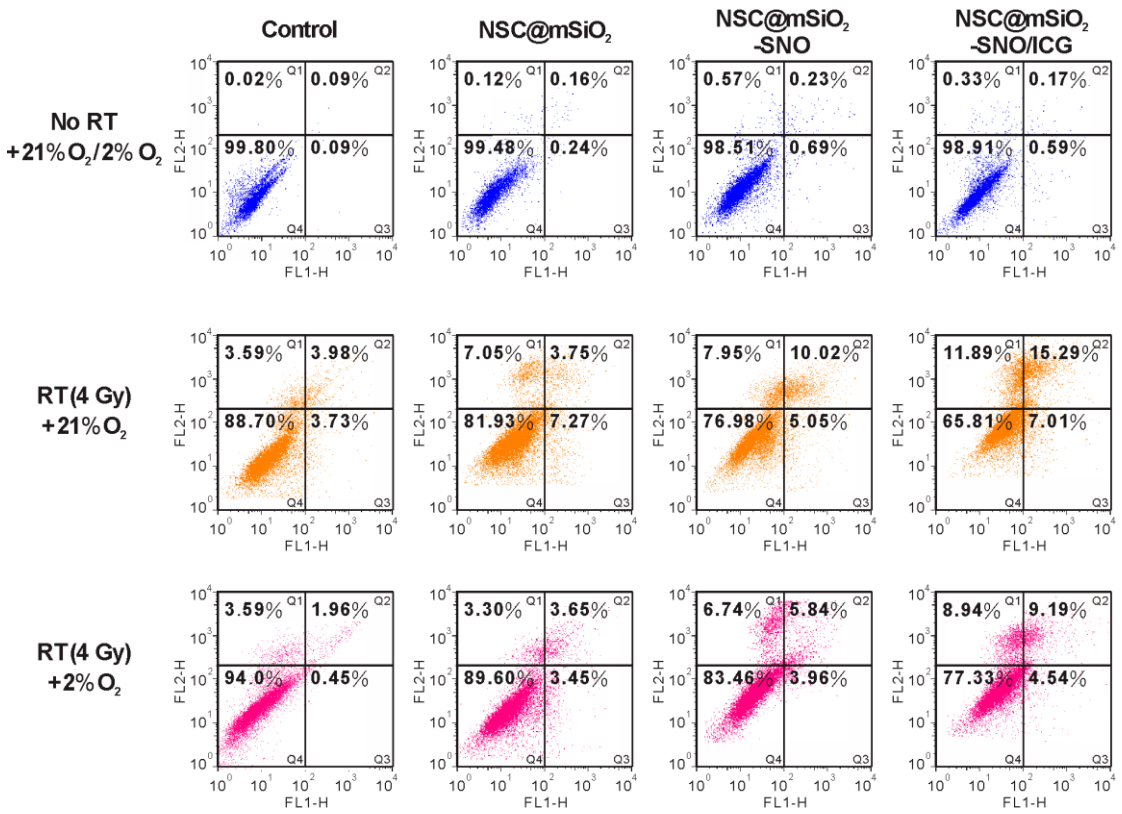

Figure S23. Flow cytometry plots for apoptosis and necrosis of 4T1 cells subjected to 4Gy X-ray radiations after 24 h normoxic (21% O_2) and hypoxic (2% O_2) incubation with different treatments of DI water (Control), NSC@mSiO_2, NSC@mSiO_2-SNO and NSC@mSiO_2-SNO/ICG, compared to the same sample treatments without X-ray radiation.

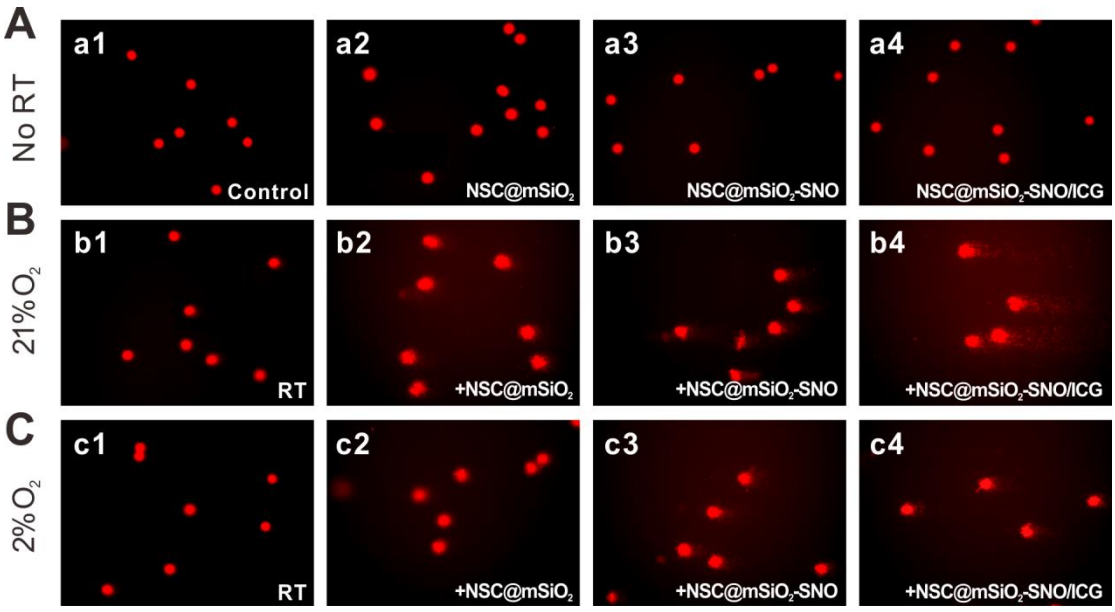

Figure S24. Comet images for DNA damage observation of 4T1 cells under normoxic (21% O_2) or hypoxic (2% O_2) conditions after 4Gy X-ray radiations with different treatments of DI water (Control), NSC@mSiO_2, NSC@mSiO_2-SNO and NSC@mSiO_2-SNO/ICG, compared to the same sample treatments without X-ray radiation.

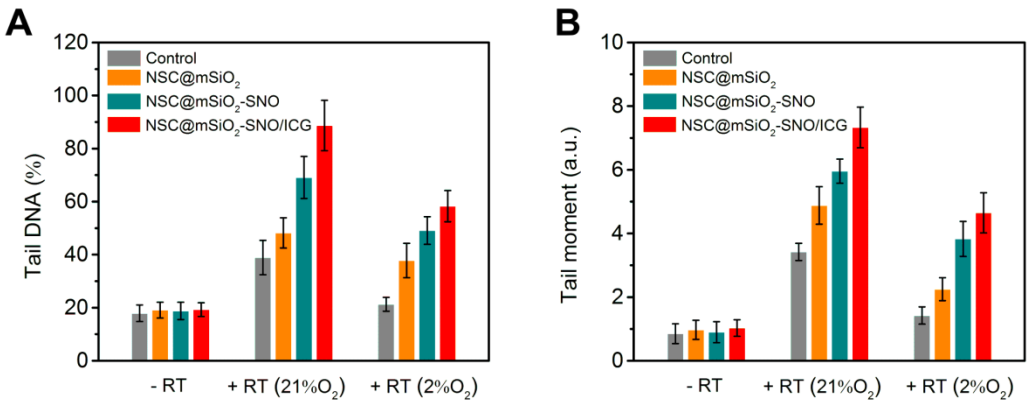

Figure S25. Tail DNA (%) **(A)** and tail moment (a.u.) **(B)** for quantification of DNA damage observation in Figure S16 under normoxic (21% O_2) or hypoxic (2% O_2) conditions after 4Gy X-ray radiations with different treatments of DI water (Control), NSC@mSiO_2, NSC@mSiO_2-SNO and NSC@mSiO_2-SNO/ICG, compared to the same sample treatments without X-ray radiation. More than 500 comets were analyzed in each experiment.

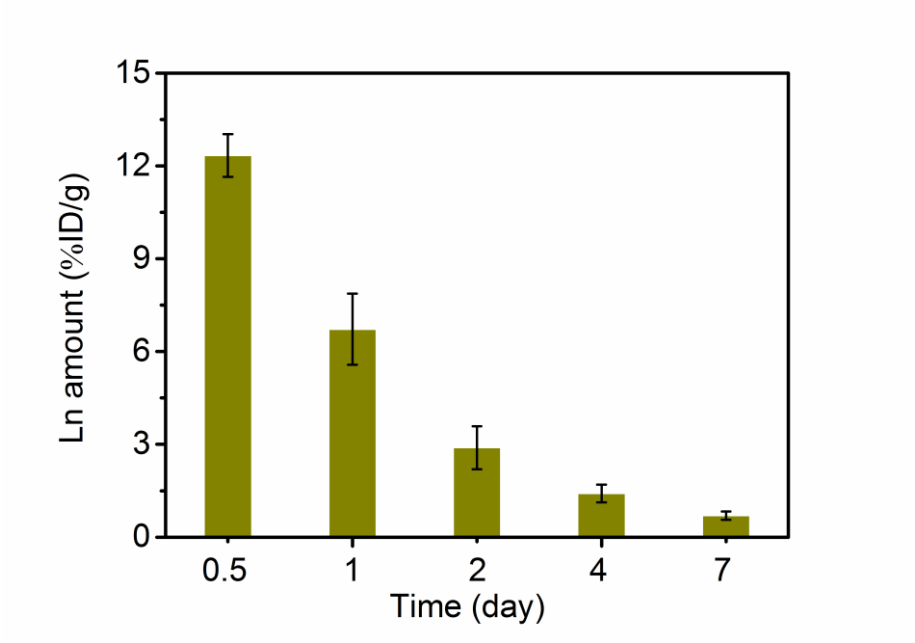

Figure S26. Time-dependent excretion data of Ln amount in the urine of the mice at different time points after intravenous injection with NSC@mSiO_2-SNO/ICG NPs.

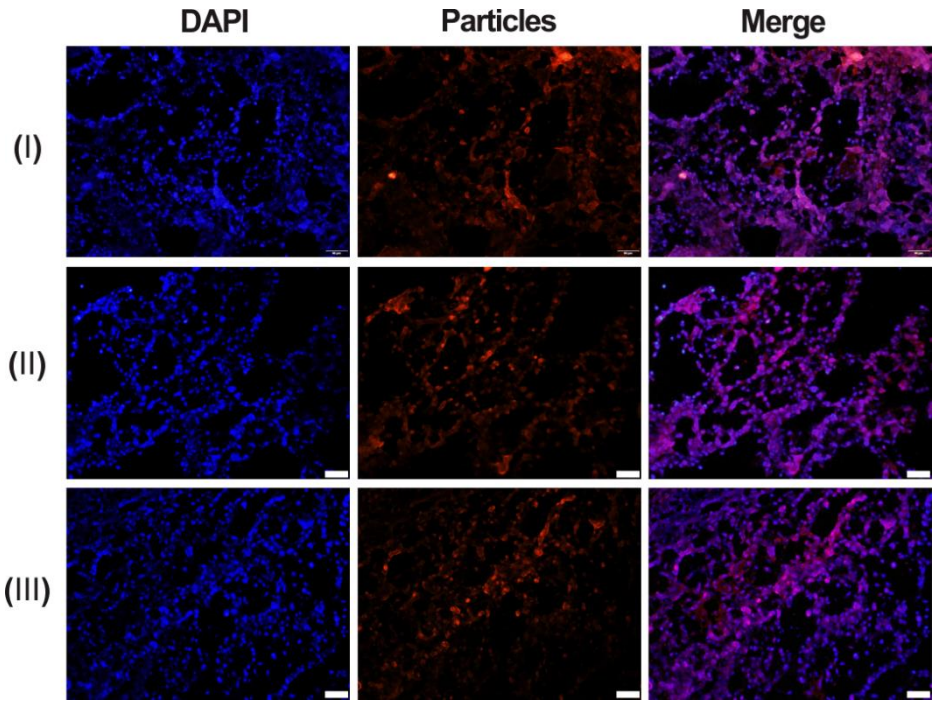

Figure S27. *Ex vivo* immunofluorescence images of tumor slices from the mice after 24 intravenous injection of NPs (scale bars = 50 μm).I: NSC NPs; II: NSC@mSiO_2-SNO NPs; III: NSC@mSiO_2-SNO/ICG NPs.

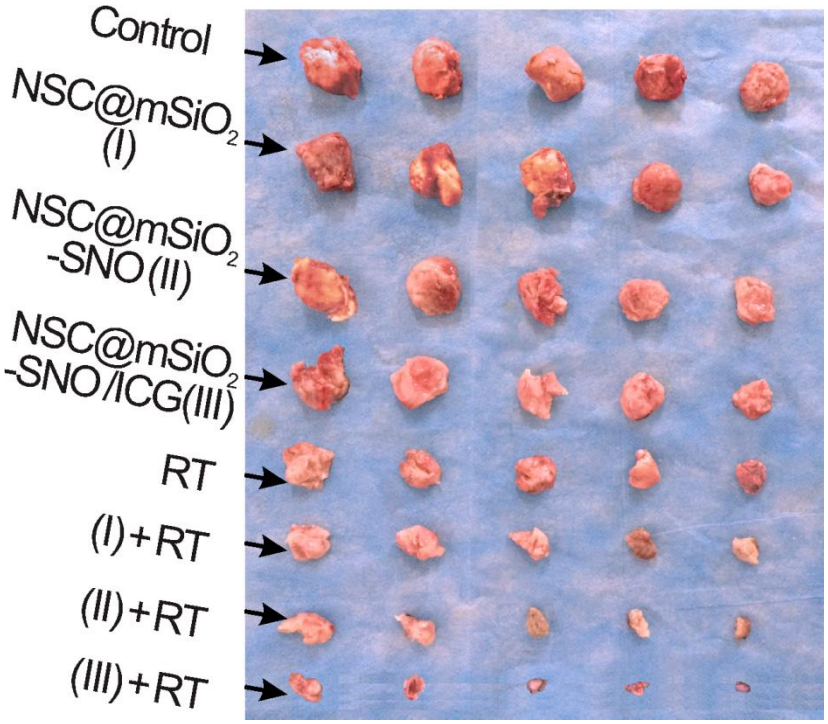

Figure S28. Representative photos of harvested tumors from mice at day 14 after different treatments (n = 5).

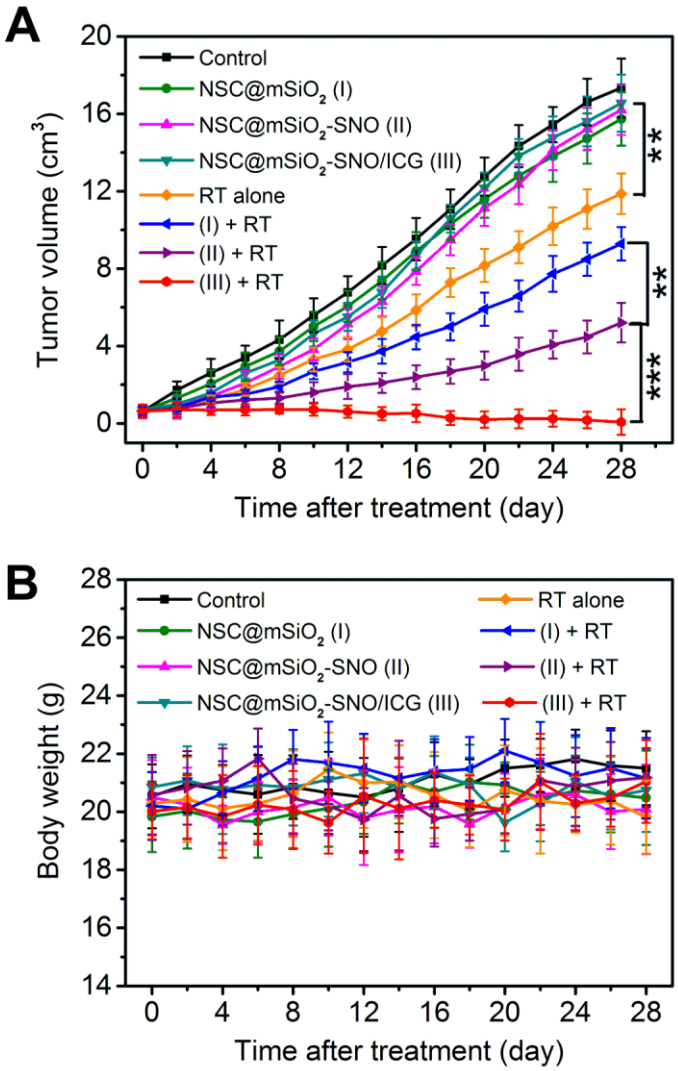

Figure S29. Long-term tumor inhibition curves **(A)** and corresponding body weights **(B)** of 4T1 tumor-bearing mice after different treatments at day 28 (n = 5).

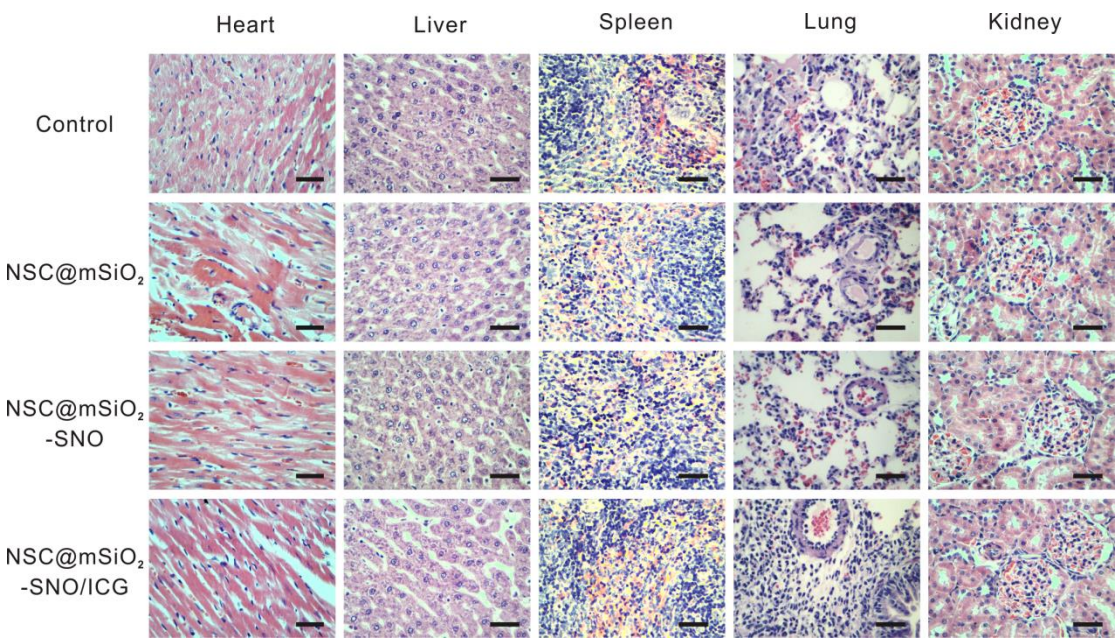

Figure S30. H&E-stained tissue sections of major organs including heart, liver, spleen, lung and kidney of mice after intravenous injection of saline (Control), NSC@$mSiO_2$, NSC@$mSiO_2$-SNO and NSC@$mSiO_2$-SNO/ICG (25 mg/kg, 100 μL) at 14th day. Scale bars are 100 μm.

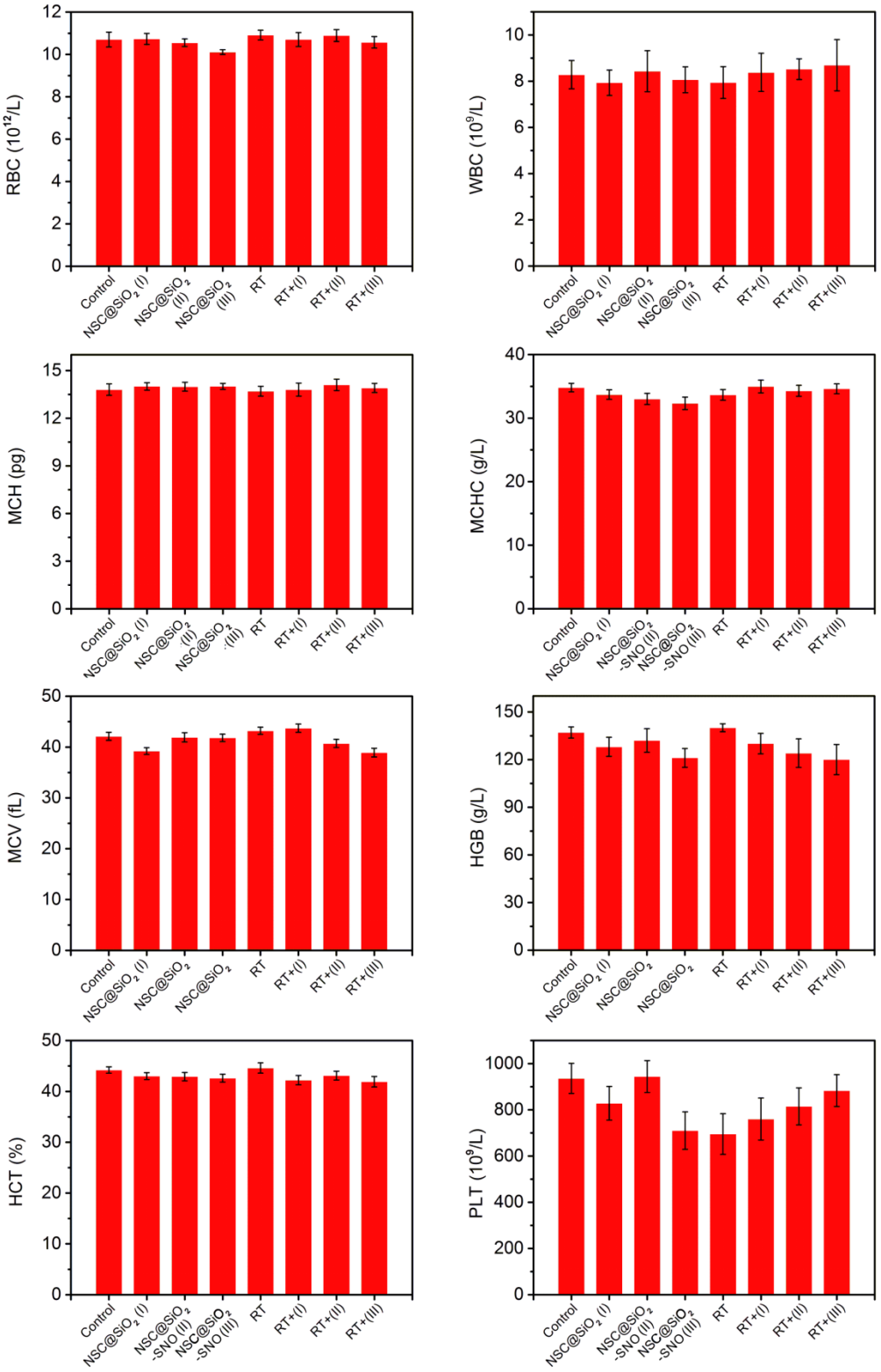

Figure S31. Hematology data obtained from the mice after various treatments by intravenous injection of different samples (25 mg/kg, 100 μL) at day14, with 100 μL saline injection as control. Error bars indicate standard deviations (SD) (n=3).

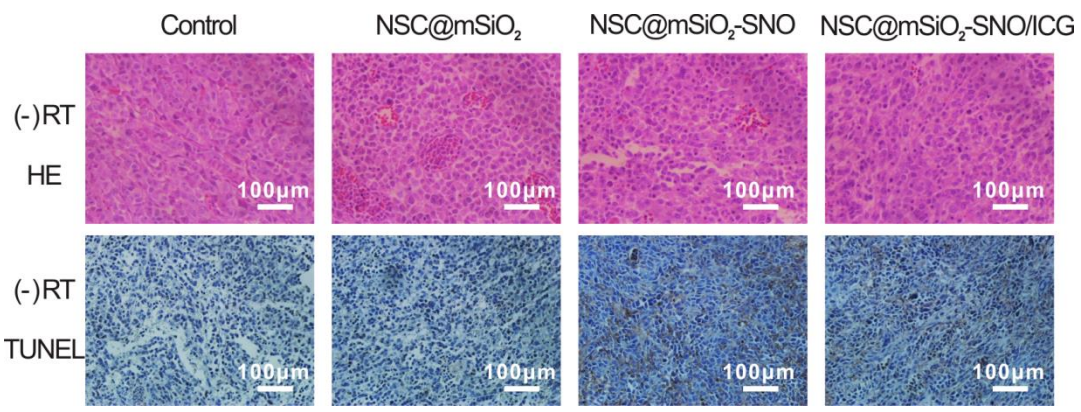

Figure S32. H&E and TUNEL staining assays of tumor tissues collected at day 14 after different treatments without RT for histological observation and apoptosis detection. Scale bars are 100 μm.

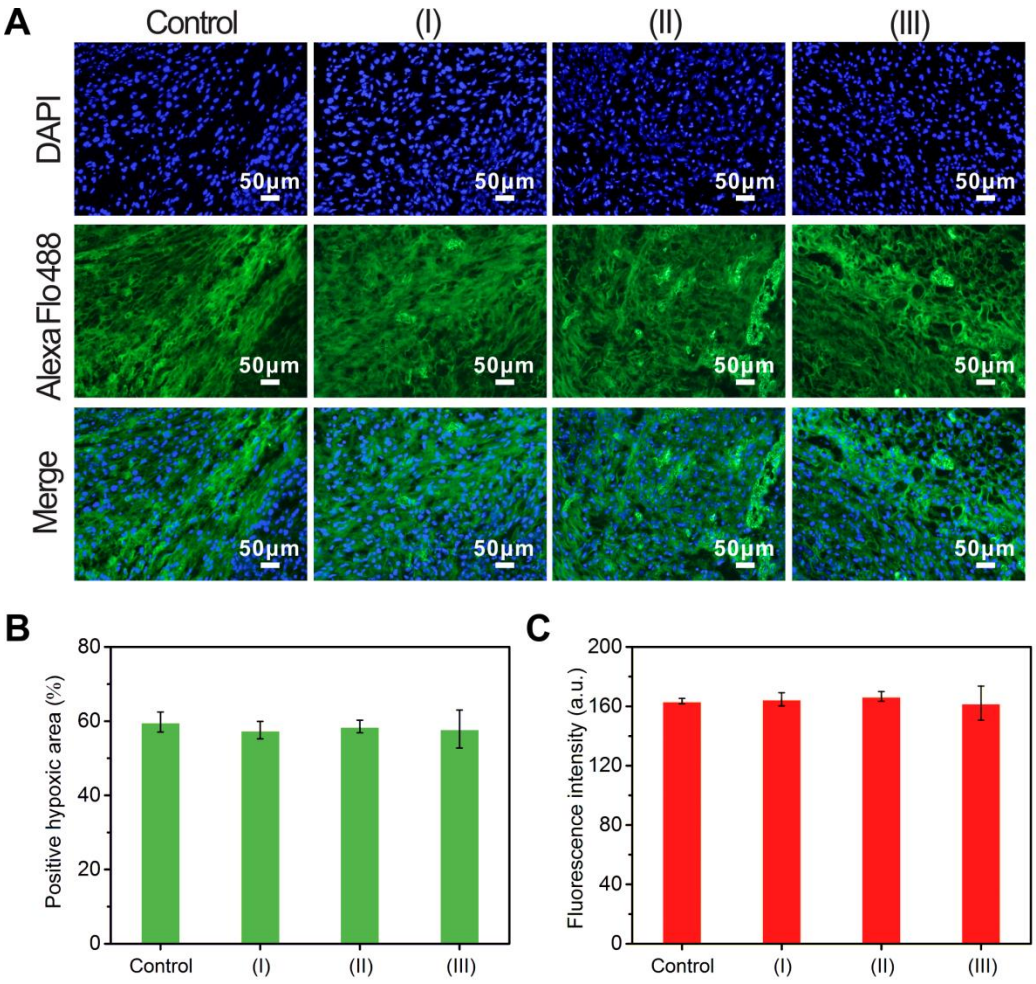

Figure S33. *Ex vivo* immunofluorescence staining images **(A)** of tumor slices collected at day 14 after different treatments without RT. Semiquantitative analysis of positive hypoxic regions **(B)** and corresponding fluorescence intensities **(C)** shown in (A). (I): NSC@mSiO_2; (II): NSC@mSiO_2-SNO; (III): NSC@mSiO_2-SNO/ICG.

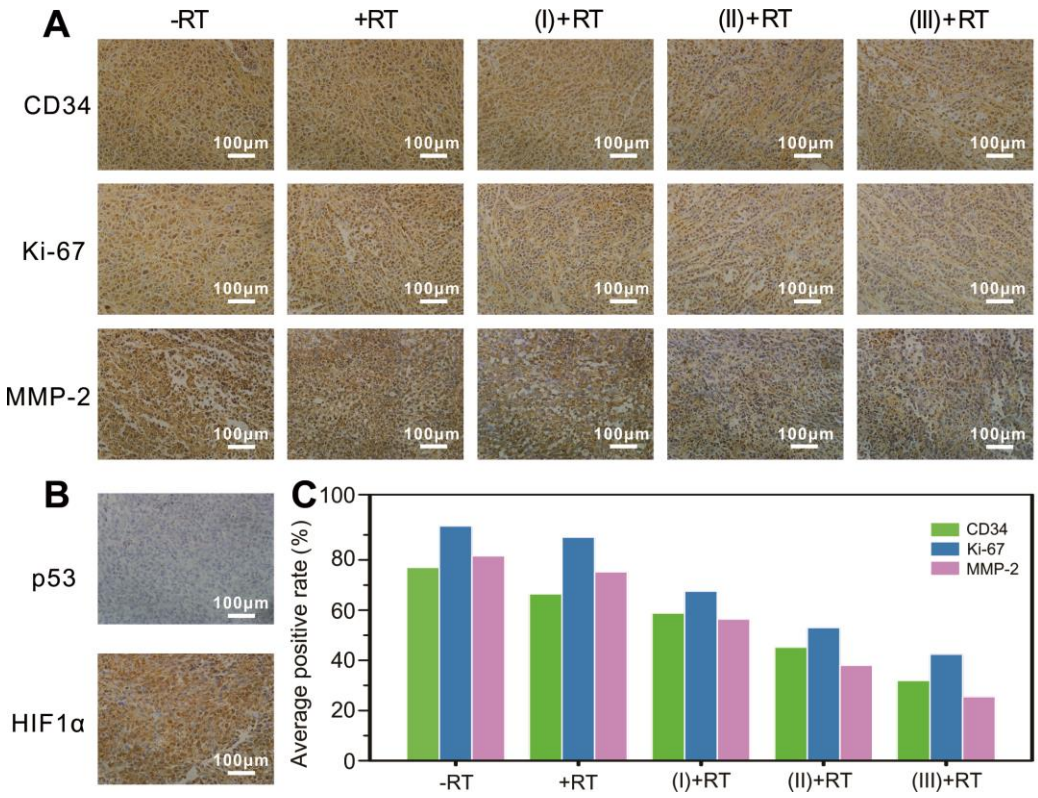

Figure S34. Immuno-histochemical analysis **(A)** and average positive rates **(C)** for CD34, Ki-67 and MMP-2 from 4T1 tumors with different treatments: (I) NSC@mSiO_2, (II) NSC@mSiO_2-SNO and (III) NSC@mSiO_2-SNO/ICG. Representative images of p53 and HIF1α for non-irradiated groups **(B)**. Scale bar corresponds to 100 μm.

Table S1. Pore size, pore volume and BET surface area of the samples.

Sample	Pore size (nm)	Pore volume ($cm^3\ g^{-1}$)	BET surface area ($m^2\ g^{-1}$)
NSC@$mSiO_2$	4.5	0.99	347
NSC@$mSiO_2$ -SNO	4.0	0.93	321
NSC@$mSiO_2$-SNO/ICG	3.6	0.79	276

Table S2. The efficiency (η) of the NSC@$mSiO_2$-SNO/ICG-induced X-PDT at various X-ray radiation dose (D).

D (Gy)	$b_m - b_c$	$q_m - q_c$	η
1	7.97	21.24	13.45
2	21.76	31.37	11.95
4	28.94	58.82	10.01
6	34.26	67.99	7.76
8	41.40	72.81	6.48

Table S3. Tail DNA, tail length and tail moment in Figure 5D.

Group	Tail DNA (%)	Tail length (pix)	Tail moment (a.u.)
1	38.9 ± 6.51	5.61 ± 0.62	3.42 ± 0.27
2	48.2 ± 5.70	8.87 ± 1.92	4.88 ± 0.59
3	69.1 ± 7.92	11.08 ± 1.32	5.96 ± 0.38
4	88.7 ± 9.51	16.35 ± 2.98	7.33 ± 0.64
5	21.3 ± 2.57	5.03 ± 0.86	1.42 ± 0.27
6	37.8 ± 6.52	6.30 ± 1.01	2.25 ± 0.36
7	49.1 ± 5.23	9.96 ± 2.71	3.83 ± 0.55
8	58.3 ± 5.91	12.18 ± 2.25	4.65 ± 0.63

Group 1-4: 21% O_2; RT, RT+ NSC@mSiO_2 NPs, RT+ NSC@mSiO_2-SNO NPs, RT + NSC@mSiO_2-SNO/ICG NPs, respectively.

Group 5-8: 2% O_2; RT, RT+ NSC@mSiO_2 NPs, RT+ NSC@mSiO_2-SNO NPs, RT + NSC@mSiO_2-SNO/ICG NPs, respectively.